Structural Engineering and Mechanics, *Vol. 52, No. 1 (2014) 173-203*
DOI: http://dx.doi.org/10.12989/sem.2014.52.1.173

Dynamic analysis of bridge girders submitted to an eccentric moving load

Ricardo F. Vieira*, Diego Lisi[a] and Francisco B. Virtuoso[b]

Department of Civil Engineering, Arquitecture and Georesources, Instituto Superior Técnico, Universidade de Lisboa, Av. Rovisco Pais 1049-001 Lisboa, Portugal

(Received January 4, 2014, Revised June 28, 2014, Accepted July 15, 2014)

Abstract. The cross-section warping due to the passage of high-speed trains can be a relevant issue to consider in the dynamic analysis of bridges due to (i) the usual layout of railway systems, resulting in eccentric moving loads; and (ii) the use of cross-sections prone to warping deformations. A thin-walled beam formulation for the dynamic analysis of bridges including the cross section warping is presented in this paper. Towards a numerical implementation of the beam formulation, a finite element with seven degrees of freedom is proposed. In order to easily consider the compatibility between elements, and since the coupling between flexural and torsional effects occurs in non-symmetric cross-sections due to dynamic effects, a single axis is considered for the element. The coupled flexural-torsional free vibration of thin-walled beams is analysed through the presented beam model, comparing the results with analytical solutions presented in the literature. The dynamic analysis due to an eccentric moving load, which results in a coupled flexural-torsional vibration, is considered in the literature by analytical solutions, being therefore of a limited applicability in practice engineering. In this paper, the dynamic response due to an eccentric moving load is obtained from the proposed finite element beam model that includes warping by a modal analysis.

Keywords: thin-walled beam dynamics; warping; eccentric moving load; lateral-torsional vibrations

1. Introduction

The structural behaviour of a bridge girder can be analyzed as a thin-walled beam and therefore one-dimensional models, properly enriched to consider three-dimensional effects, can advantageously be adopted for its analysis when compared with sophisticated shell finite element models. In fact, shell models not only require more data towards the definition of the model, which remains sometimes undefined at a designing stage, but also produce a considerable amount of data to post-process and interpret that can mislead the analysis of a less experienced engineer.

On the other hand, the use of beam models not sufficiently refined, i.e., not considering deformation modes of higher order, fails to consider three-dimensional structural effects, which can be significative in high-speed railway bridges given the usual layout adopted for the railway

*Corresponding author, Ph.D., E-mail: ricardo.figueiredo.vieira@tecnico.ulisboa.pt
[a]MsC., E-mail: diegolisi1987@gmail.com
[b]Ph.D., E-mail: francisco.virtuoso@tecnico.ulisboa.pt

http://www.techno-press.org/?journal=sem&subpage=8 ISSN: 1225-4568 (Print), 1598-6217 (Online)

lanes. In fact, railway lanes have often an eccentricity in relation to the shear centre of the bridge cross-section, which implies to consider the cross-section torsion, warping and distortion in the analysis.

Therefore, the use of a one-dimensional model for the dynamic analysis of railway bridge girders should be able to consider the most relevant 3D structural behaviour, considering both the girder cross-section geometry and the lane layout.

For an arbitrary cross section geometry the cross section shear centre, centroid and mass centre do not coincide, resulting in a coupled system of dynamic equations that has associated a triple coupling between flexural and torsional vibrational modes. Hence, this coupling has to be considered in the beam model either in a free vibration analysis or when the beam is subjected to moving loads. Moreover, for an accurate analysis of the problem, in addition to the cross section warping, the cross section shear deformation and rotary inertia should be included in the analysis.

The analysis of coupled free vibrations in beams considering these effects is a subject where extensive work has been developed. One of the earliest works to include warping effects was addressed in Vlasov (1961), Gere (1954, 1958), where an analytical solution for the free vibration both for symmetric and mono-symmetric cross-sections was given.

A method commonly adopted for the solution of the coupled equations is the dynamic stiffness matrix method, which is often referred as an exact method inasmuch it considers the analytical solutions of the governing equations to derive a dynamic matrix (frequency dependent) that includes both mass and stiffness properties of the element, allowing to obtain natural frequencies, Banerjee (1989); a general approach for the dynamic stiffness formulation is presented in Banerjee (1997).

The coupled vibration for a *Timoshenko* beam was studied through the dynamic stiffness method, deriving from the solution of the respective equations of motion analytical expressions for the corresponding matrix, Banerjee and Williams (1992).

A dynamic stiffness matrix that considers the triple coupling, but neglects warping was derived by Friberg (1983). The effect of warping was included in Hallauer and Liu (1982), Friberg (1985), Dokumaci (1987), Bishop *et al.* (1989), Banerjee *et al.* (1996), Tanaka and Bercin (1997) regarding the evaluation of free vibration frequencies of thin-walled beams, being concluded that the effect of warping stiffness on natural frequencies is significant.

More recently, a dynamic matrix for thin-walled beam-columns subjected to eccentrically axial loads was proposed in Kim *et al.* (2003), being considered the cross section warping and the coupling due to shear deformation in Kim and Kim (2005). The free vibration of thin-walled open sections considering the coupling between axial (due to restraining the axial displacement in a point different from the centroid), bending and torsional vibrations is considered in Chen (2008) through the formulation of a seven degree freedom beam element. The free vibrations of curved beams were studied analytically including the effects of rotary inertia, shear and axial deformations in Zhu *et al*. (2013).

The coupled free vibrations of thin-walled beams was also studied analytically in Tanaka and Bercin (1999), Arpaci *et al*. (2002, 2003), Prokic (2005) where the effect of neglecting the rotary inertia as well as the cross section warping on the accuracy of results was analysed; the coupling effect due to warping, including the thin-walled beam shear deformation, was addressed in Prokic (2006).

The analysis of beams subjected to moving loads is a topic that has been extensively studied since the early work of Timoshenko (1974), Fryba (1999) and more recently in Olsson (1985, 1991). Nevertheless, the works dealing with the combined lateral-torsion of beams considering the cross section warping under moving loads are relatively limited, Michaltsos *et al*. (2005).

However, and in particular for high-speed trains, the repeated action of axle loads can lead to resonance vibration problems, Fryba (2001). Hence, regarding the dynamic analysis of railway bridges for high-speed trains, the influence of the load eccentricity together with its repeated action at a high-speed should be taken into account.

This dynamic analysis can be performed through a 3D finite element model, Ju and Lin (2003), Lee and Yhim (2005), Podworna (2011a, b). However, the analysis of moving loads along the girder through the use of a beam model capable to incorporate such 3D effects would be simpler, less consuming, and will allow a more clear interpretation of the phenomena given its uncoupled nature. Beam models have already been successfully adopted for the analysis of relevant bridge dynamic topics Mohammad (2013); however, the response due to moving loads does not consider the effect of coupling between bending and torsion Yang *et al*. (1997), Li and Su (1999), Garinei and Risitano (2008), Ichikawa *et al*. (2000), Piccardo and Tubino (2012).

To the best knowledge of the authors, one of the works considering the coupling between bending and torsion through a beam model, simultaneously with a moving load, was presented in Michaltsos *et al*. (2005). This study relies on the analytical solution of the coupled equations of motion derived from the application of an eccentric moving load, which is obtained by considering the separation of variables and using harmonic functions, as in the classic solutions of the problem; however, since it relies on an analytical solution, its use to more general structural systems is somewhat limited.

A model for the dynamic analysis of the coupled torsional-bending vibrations of thin-walled beams subjected to a "high-speed" moving load through a one-dimensional model that considers the cross-section warping is presented in this paper. The model is developed under the framework of the finite element method through an approximation of the displacement field along the longitudinal axis, allowing to be efficiently adopted for the analysis of railway bridge girders. The cross-section is considered to be in-plane undeformable, being the cross section warping defined according to *Vlasov's* theory. The beam model is subjected to a moving load, being the corresponding mass considered to be small relatively to the mass of the girder. Moreover, although the objective is to consider the effect of high-speeds trains, the work is focused only in terms of modeling the torsional bending coupling together with a moving load, representing the train traveling at high speed, disregarding other relevant issues specific to the carriage modeling, in particular the vehicle-structure interaction.

2. Thin-walled beam formulation

A beam-like model considering the warping of the thin-walled cross-section will be developed in this section according to the *Vlasov* theory, in order to obtain a set of equations describing both the static and the dynamic equilibrium of the bridge girder. The beam governing equations are derived according to the small displacement hypothesis for a linear, elastic and isotropic material. The cross-section is admitted to be in-plane rigid, being the shear strain of the middle surface of the open cross-section neglected. The beam can have a generic cross-section geometry, being adopted the most common layouts for civil engineering applications.

2.1 Displacement field

The cross-section layout considered in this formulation is admitted to be constituted by a set of

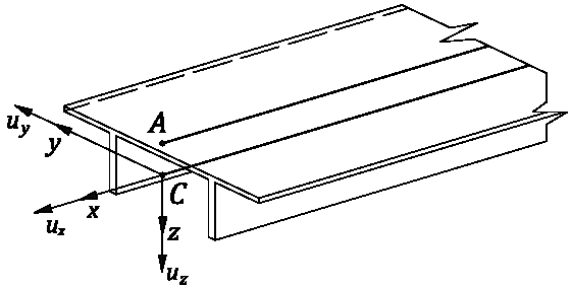

Fig. 1 Thin-walled beam element

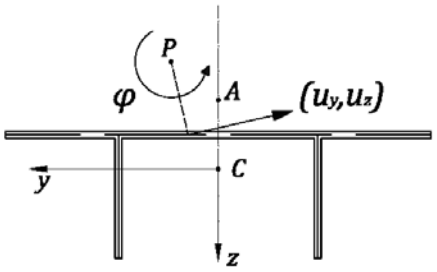

Fig. 2 Cross-section rotation around a generic point

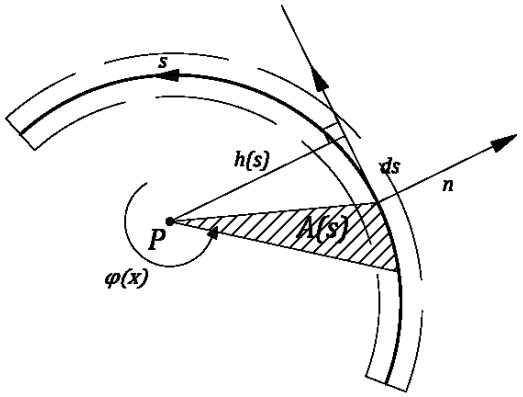

Fig. 3 Rotation of a thin-walled sector

rectilinear wall segments forming a generic shape, either of open or closed profile. A global reference frame $O(x,y,z)$ is adopted for the thin-walled beam element, where x represents the longitudinal axis of the beam and y, z the principal transverse axes, being represented in Figs. 1 and 2; a local right oriented reference frame $O(x,y,z)$ is considered for each wall element, where the coordinate s defines the coordinate running along the midline of the cross section, and n corresponds to the perpendicular direction to the wall of each element. The coordinates s and n are illustrated in Fig. 3 for a generic wall sector. The surface defined by the cartesian pair (x,s) corresponds to the cross section middle surface.

The displacement field is referred to a generic point $P=(y_P,z_P)$, being η x) the corresponding axial displacement and $\xi_y(x)$ and $\xi_z(x)$ the respective transverse displacements along the y and z direction, respectively. The transverse displacement of a cross-section is described by two body translations ξ_y and ξ_z along the y and z axis, respectively, and a rigid twist rotation φ around a generic point $P=(y_P,z_P)$ as illustrated in Figs. 1 and 2. The in-plane displacement components are given by

$$u_y(x,y,z)=\xi_y(x)-\left(z-z_P\right)\varphi(x) \text{ and } u_z(x,y,z)=\xi_z(x)+\left(y-y_P\right)\varphi(x) \tag{1}$$

The beam axial displacement is defined according to the assumed hypotheses as follows,

$$u_x(x,y,z)=\eta(x)-\left(y-y_P\right)\xi_y'(x)-\left(z-z_P\right)\xi_z'(x)-\omega_P(s)\varphi'(x) \tag{2}$$

which corresponds to the *Vlasov's* kinematical description, being the warping function defined

through the sectorial coordinate represented in Fig. 3, properly corrected so as to consider cross-sections with a closed profile (see Cedolin 1996). The warping is thus defined as follows

$$\omega_P(s) = \int_0^s \left(h_P(s) - \psi / t \right) ds + c \text{ with } \psi = \frac{2\Omega_m}{\oint ds / t} \tag{3}$$

where $h_P(s)$ is the distance from the rotation pont P to the tangent of s, $_P(s)$ is the sectorial coordinate relative to P, t is the thickness of the section wall and Ω_m the area delimited by the midline of the closed profile. The constant c can be obtained by imposing the following condition:

$$\oint \omega_P(s) t ds = 0 \tag{4}$$

The coefficient Ω_m in Eq. (3) cancels for open cross-sections and the warping coordinate is reduced to the *Vlasov* sectorial coordinate, Vlasov (1961). A method that obtains the warping function and the location of the shear centre in a single step, which was developed in Attard (1987) and implemented in a numerical code in Lisi (2012), is adopted for the developed model. The method is independent of the axes' selection, of the elastic centre location and of the principal axes direction, which are calculated in a systematic way. The warping constant is easily evaluated by using the warping function distribution along the section profile by integration of linear functions.

2.2 Deformation field

The deformation field is defined according to the compatibility conditions, as follows

$$\varepsilon_x = \frac{\partial u_x}{\partial x} \text{ and } \gamma_{xs} = \frac{\partial u_x}{\partial s} + \frac{\partial u_s}{\partial x} \tag{5}$$

which considering the displacement definition in Eq. (2) yields the following deformation components

$$\varepsilon_x = \eta'(x) - \left(y - y_P \right) \xi_y''(x) - \left(z - z_P \right) \xi_z''(x) - \omega_P(s) \varphi''(x) \tag{6}$$

$$\gamma_{xs} = 2n\varphi'(x) \tag{7}$$

being the corresponding stress field obtained by the following uniaxial constitutive relations

$$\sigma_x = E\varepsilon_x \text{ and } \tau_{xs} = G\gamma_{xs} \tag{8}$$

where E is the elasticity modulus and G the shear modulus.

Under the considered assumptions, the bending and the non-uniform torsion of the beam do not consider the shear deformation of the cross-section due to flexure and hence the corresponding tangential stresses can only be obtained through local equilibrium equations. The tangential stresses due to distortion are reduced to the contribution of the uniform torsion. The corresponding set of internal forces are obtained by integrating the stress field components over the beam cross-section, being summarized in Table A.2 presented in appendix.

2.3 Beam equations of motion

The beam dynamic equilibrium equations are derived according to the variational principles in

mechanics by defining a stationary value for the definite integrals corresponding to the beam energy. This is generally known as the Hamilton principle, which allows to derive the equations of motion. The beam energy is expressed as a functional of the displacement field, which is enforced to become stationary through

$$\int_{t_1}^{t_2} \delta\left(E_k - V\right) dt = \int_{t_1}^{t_2} \left(\frac{\partial E_k}{\partial q_i}\delta q_i + \frac{\partial E_k}{\partial \dot{q}_i}\delta \dot{q}_i + \frac{\partial E_k}{\partial \dot{q}_i'}\delta \dot{q}_i' - \frac{\partial V}{\partial q_i}\delta q_i - \frac{\partial V}{\partial q_i'}\delta q' - \frac{\partial V}{\partial q_i''}\delta q_i'' \right) dt = 0 \tag{9}$$

where the dot and the prime express the time and spatial (with respect to the x coordinate) derivation, respectively. E_k represents the beam kinetic energy of the structure, V the potential energy, which is calculated by the relation between the strain energy U and the work of conservative external forces W as $V=U-W$; the variation δq_i represents the generalised coordinate relative to the i-degree of freedom, being kinematical compatible. Integrating the velocity dependent terms of Eq. (9), the following Lagrangian equations for the generalized virtual displacements are derived

$$\int_{t_1}^{t_2} \left(\frac{\partial E_k}{\partial q_i}\delta q_i - \frac{\partial E_k}{\partial \dot{q}_i}\delta q_i - \frac{\partial E_k}{\partial \dot{q}_i'}\delta q_i' - \frac{\partial V}{\partial q_i}\delta q_i - \frac{\partial V}{\partial q_i'}\delta q' - \frac{\partial V}{\partial q_i''}\delta q_i'' \right) dt = 0 \tag{10}$$

The application of Eq. (10) to the formulation of the thin-walled beam governing requires the definition of the corresponding beam energy. For an elastic linear analysis and taking in account that the external forces are conservatives, the potential energy is given as follows

$$V = U - W \text{ with } U = \frac{1}{2}\left(E\varepsilon_x^2 + G\gamma_{xs}^2\right) \tag{11}$$

where U represents the the beam deformation energy obtained by considering the deformation field defined in Eqs. (6)-(7). The axial component of the strain energy per unit length is obtained by substituting the Eq. (6) in the first term of Eq. (11) as follows

$$\frac{1}{2}\int_A E\varepsilon_x^2\, dA = \frac{1}{2}E\left[\eta' - \xi_y'' - \xi_z'' - \varphi''\right] \begin{bmatrix} A & S_y^P & S_z^P & S_\omega^P \\ S_y^P & I_y^P & I_{yz}^P & I_{y\omega}^P \\ S_z^P & I_{zy}^P & I_z^P & I_{z\omega}^P \\ S_\omega^P & I_{\omega y}^P & I_{\omega z}^P & I_\omega^P \end{bmatrix} \begin{bmatrix} \eta' \\ -\xi'' \\ -\xi_z'' \\ -\varphi'' \end{bmatrix} \tag{12}$$

while the substitution of Eq. (7) in the second term of the Eq. (11) leads to the tangential strain energy component per unit length

$$\frac{1}{2}\int_A G\gamma_{xs}^2\, dA = \frac{1}{2}\varphi' GK\varphi' \tag{13}$$

The work of the external forces is defined per unit volume as follows

$$W = p_x u_x + p_y u_y + p_z u_z \tag{14}$$

where p_x, p_y and p_z are the components of the volume load vector along the directions x, y and z,

respectively. Integrating Eq. (14) over the cross-section area, the following expression is obtained

$$\int_A \left(p_x u_x + p_y u_y + p_z u_z\right) dA = q_x \eta + q_y \xi_y + q_z \xi_z + m_\varphi \varphi - m_y \xi_y' - m_z \xi_z' - b\varphi' \tag{15}$$

The resultant line loads are summarized in the appendix Table A.3 for the generalized degrees of freedom. The energy defined in Eq. (11) is written as a *functional* of the generalized displacement functions by considering Eqs. (12)-(13) and (15). The elastic energy can be written as

$$V = \int_L F_V \left[\eta, \eta', \xi y, \xi z, \varphi, \xi_y', \xi_z', \varphi', \xi_y'', \xi_z'', \varphi''\right] dL \tag{16}$$

where the functional F_V represents the elastic energy per unit length of the beam, being defined as follows

$$\begin{aligned} F_V = {} & \frac{1}{2} E \left(\eta' A \eta' - \eta S_y^P \xi_y'' - \eta S_z^P \xi_z'' - \eta' S_\omega^P \varphi'' - \xi_y'' S_y^P + \xi_y'' I_y^P \xi_y'' + \xi_y'' I_{yz}^P \xi_y'' + \xi_y'' I_{y\omega}^P \varphi'' - \xi_z'' S_z^P \right. \\ & \left. + \xi_z'' I_{zy}^P \xi_y'' + \xi_z'' I_z^P \xi_z'' + \xi_z'' I_{z\omega}^P \varphi'' - \omega'' S_\omega^P + \omega'' I_{zy}^P \xi'' + \omega'' I_z^P \xi'' + \omega'' I_{\omega\omega}^P \varphi'' \right) + \frac{1}{2} \varphi' G K \varphi' \\ & - q_x \eta + q_y \xi_y + q_z \xi_z + m_\varphi \varphi - m_y \xi_y' - m_z \xi_z' - b\varphi' \end{aligned} \tag{17}$$

Notice that the terms in braces are referred to the four generalized displacements that represent the axial strain of the beam. The term of Eq. (13) is due to the tangential strain energy. The geometric properties of the cross-section represented in Eq. (17) are summarized in the appendix at Table A.1. The kinetic energy of the beam is defined by considering the corresponding inertial forces as follows

$$E_k = \frac{1}{2} \int_V \rho \left(\dot{u}_x^2 + \dot{u}_y^2 + \dot{u}_z^2 \right) dV \tag{18}$$

with representing the mass per unit volume and where the three components take into account the kinetic energy associated with the element motion along directions x, y and z, respectively. The displacements are those described by Eqs. (1)-(2). The kinetic energy associated with the thin-walled beam extension, bending and torsion, considering the warping of the cross-section, is defined by substituting the displacement field u_x (obtained from Eq. (2)) into the corresponding component of Eq. (18), being written as follows

$$\begin{aligned} \frac{1}{2} \rho \dot{u}_x^2 = {} & \frac{1}{2} \rho \left[\dot{\eta} - (y - y_P) \dot{\xi}_y' - (z - z_P) \dot{\xi}_z' - \omega_P \dot{\varphi}' \right]^2 = \frac{1}{2} \rho \left[\dot{\eta}^2 - \dot{\eta} (y - y_P) \dot{\xi}_y' - \dot{\eta} (z - z_P) \dot{\xi}_z' \right. \\ & - \omega_P \dot{\varphi}' - (y - y_P) \dot{\xi}_y' \dot{\eta} + \left[(y - y_P) \dot{\xi}_y' \right]^2 + (y - y_P)(z - z_P) \dot{\xi}_y' \dot{\xi}_z' + (y - y_P) \omega_P \dot{\xi}_y' \dot{\varphi}' \\ & - (z - z_P) \dot{\xi}' \dot{\eta} + (z - z_P)(y - y_P) \dot{\xi}_z' \dot{\xi}_y' + \left[(z - z_P) \dot{\xi}_z' \right]^2 + (z - z_P) \omega_P \dot{\xi}_z' \dot{\varphi}' - \omega_P \dot{\varphi}' \dot{\eta} \\ & \left. + \omega_P (y - y_P) \dot{\varphi}' \dot{\xi}_y' + \omega_P (z - z_P) \dot{\varphi}' \dot{\xi}_z' + \left(\omega_P \dot{\varphi}' \right) \right] \end{aligned} \tag{19}$$

The kinematic contribution of the transverse displacements is derived by considering Eq. (1), being written as follows

$$\frac{1}{2}\rho\left(\dot{u}_y^2+\dot{u}_z^2\right)=\frac{1}{2}\rho\left[\dot{\xi}_y^2-2\dot{\xi}_y\left(z-z_P\right)\dot{\varphi}+\left[\left(z-z_P\right)\dot{\varphi}\right]^2+\dot{\xi}_z^2-2\dot{\xi}_z\left(y-y_P\right)\dot{\varphi}+\left[\left(y-y_P\right)\dot{\varphi}\right]^2\right] \quad (20)$$

The integration over the cross-section of the Eqs. (19)-(20) leads to the energy functional F_{Ek}, which allows to obtain the beam kinetic energy written as follows

$$E_k=\int_0^L F_{E_k}\left[\dot{\eta},\dot{\xi}_y,\dot{\xi}_z,\dot{\varphi},\dot{\xi}_y',\dot{\xi}_z',\dot{\varphi}'\right]dL \quad (21)$$

where the energy per unit length is given by

$$\begin{aligned}F_{E_k}=&\frac{1}{2}\rho\big(A\dot{\eta}^2-\dot{\eta}S_y^P\dot{\xi}_y'-\dot{\eta}S_z^P\dot{\xi}_z'-\dot{\eta}S_\omega^P\dot{\varphi}'-S_y^P\dot{\xi}_y'\dot{\eta}+I_y^P\dot{\xi}'^2+I_{yz}^P\dot{\xi}_y'\dot{\xi}_z'+I_{y\omega}^P\dot{\xi}_y'\dot{\varphi}'\\&-S_z^P\dot{\xi}_z'\dot{\eta}+I_{zy}^P\dot{\xi}_z'^2\dot{\xi}_y'^2+I_z^P\dot{\xi}_z'^2+I_{z\omega}^P\dot{\xi}_z'\dot{\varphi}'-S_\omega^P\dot{\varphi}'\dot{\eta}+I_{\omega y}^P\dot{\varphi}'\dot{\xi}_y'+I_{\omega z}^P\dot{\varphi}'\dot{\xi}_z'+I_{\omega\omega}^P\dot{\varphi}'^2\\&A\dot{\xi}_y'^2-2\dot{\xi}_yS_z^P\dot{\varphi}+I_z^P\dot{\varphi}^2+A\dot{\xi}_z'^2+2\dot{\xi}_zS_y^P\dot{\varphi}+I_y^P\dot{\varphi}^2\big)\end{aligned} \quad (22)$$

The functional of Eq. (22) takes into account the inertial forces due to the motion of the beam and depends on the generalized velocities. The equation (10) is rearranged considering (i) $\delta\eta$, $\delta\eta'$ for the axial problem, (ii) $\delta\xi_y,\delta\xi_y',\delta\xi_y''$ and $\delta\xi_z,\delta\xi_z',\delta\xi_z''$ for the bending in the two directions and (iii) $\delta\varphi,\delta\varphi',\delta\varphi''$ for the torsion of the beam. The dynamic equilibrium equations are obtained by the integration by parts of Eq. (10) considering the definition of the functionals given in Eqs. (16) and (22), being the resulting set of differential equations written in Eqs. (23)-(26) for the 7 degrees of freedom represented in Fig. 4. The equations are represented in an uncoupled form by considering the bending and the axial effects of the beam referred to the elastic centre axis and the twist with respect to the shear centre axis:

Axial displacement

$$-\rho A\frac{\partial^2\eta}{\partial t^2}+EA\frac{\partial^2\eta}{\partial x^2}+q_x=0 \quad (23)$$

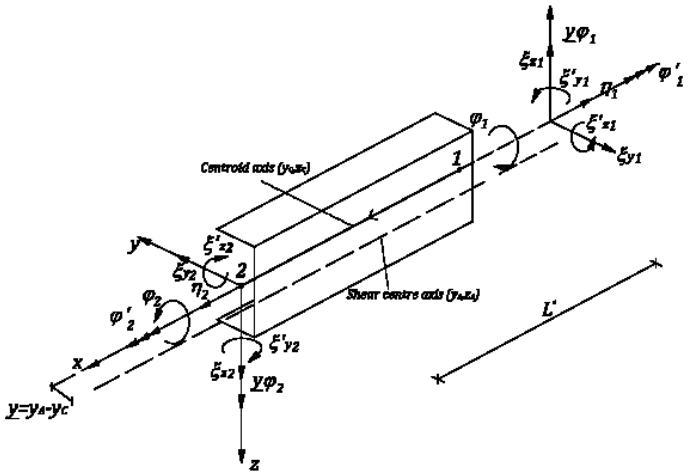

Fig. 4 Beam model model

Bending in (x, y) plane

$$\frac{\partial^2 M_y}{\partial x^2}+\frac{\partial m_y}{\partial x}+q_y-\rho A\frac{\partial^2 \xi_y}{\partial t^2}+\rho S_z^A\frac{\partial^2 \varphi}{\partial t^2}+\rho I_y\frac{\partial^2 \xi_y''}{\partial t^2}=0 \tag{24}$$

Bending in (x, y) plane

$$\frac{\partial^2 M_z}{\partial x^2}+\frac{\partial m_z}{\partial x}+\rho I_y\frac{\partial^2 \xi_z''}{\partial t^2}\frac{\partial V_z}{\partial x}+q_z-\rho A\frac{\partial^2 \xi_z}{\partial t^2}-\rho S_y^A\frac{\partial^2 \varphi}{\partial t^2}=0 \tag{25}$$

Torsion

$$T=\rho I_{\omega\omega}\frac{\partial^2}{\partial t^2}\left(\frac{\partial \varphi}{\partial x}\right)+\frac{\partial M_\varphi}{\partial x}+T_S+b \tag{26}$$

$$\frac{dT}{dx}-\rho\left(I_y^A+I_z^A\right)\frac{\partial \varphi^2}{\partial t^2}+\rho S_z^A\frac{\partial^2 \xi_y}{\partial t^2}-\rho S_y^A\frac{\partial^2 \xi_z}{\partial t^2}+m_\varphi=0 \tag{27}$$

where the superscript A refers to the shear centre; the cross-section properties and the beam internal forces are defined in Tables A.1, A.2 and A.3. The differential equations that represent the static equilibrium of thin-walled beams are obtained by considering the time-dependent derivatives of the generalized displacement to be null.

In the dynamic equilibrium Eq. (26), where all inertial contributions are considered, bending and torsion are coupled through the terms S_z^A and S_y^A. In fact, in thin-walled beam dynamics, although considering the cross-section kinematic's referred to the shear centre and the elastic centre, the flexural and torsional behaviour remain coupled. This coupling is a result of the rotation around $A(y_\omega z_\alpha)$ causing transverse displacements of the elastic centre, Friberg (1985).

3. Numerical model of the thin-walled beam

3.1 Finite element formulation

A finite element is derived for the solution of the governing beam differential equations for an arbitrary thin-walled cross section. The formulation of the finite element considers the displacement field interpolation functions to be also adopted as weight functions (*Galerkin* approach), in order to derive the corresponding discrete equations. In comparison to conventional beam elements this finite element considers an additional degree-of-freedom to represent the cross-section warping, being suitable for considering this effect both in static and dynamic analysis of thin-walled beams.

The main objective of this beam model is the application to the dynamic analysis of bridge girders, particularly regarding its dynamic analysis considering the warping and eccentric loads. However, the application to a static analysis was also performed in order to validate the model, being the results presented in Lisi (2012). The approximation of the displacement field for the beam finite element is defined as follows

$$\zeta^e=\begin{bmatrix}\mathbf{N} & \mathbf{H}_y^e & \dfrac{-d\mathbf{H}_y^e}{dx} & \mathbf{H}_z^e & \dfrac{-d\mathbf{H}_z^e}{dx} & \mathbf{H}_\varphi^e & \dfrac{-d\mathbf{H}_\varphi^e}{dx}\end{bmatrix}\mathbf{u}^e \tag{28}$$

with ζ^e and $\mathbf{u}^e$ defined by

$$\zeta^e = \begin{bmatrix} \eta^e & \xi_y^e & \xi_y'^e & \xi_z^e & \xi_z'^e & \varphi^e & \varphi'^e \end{bmatrix} \text{ and } \mathbf{u}^e = \begin{bmatrix} u_x^e & u_y^e & u_y^e & u_z^e & u_z^e & u_\varphi^e & u_\varphi^e \end{bmatrix}^T \quad (29)$$

where linear and *Hermite* polynomials, $\mathbf{N}^e$ and $\mathbf{H}_i^e$, respectively, are used as approximation functions in order to obtain the *continuity* and the *completeness* required for the finite element beam model. The vectors $\mathbf{u}_i^e$, with $i=x, y, z$ and φ represent the generalized vectors containing the displacements of the end nodes of the element.

The displacement field interpolation is substituted in the beam equilibrium Eqs. (23)-(26) obtained by applying the Hamilton's principle, being the resultant residue weighted by the same set of interpolation functions towards the definition of the corresponding weak formulation.

The undampened dynamic equilibrium of the thin-walled beam corresponding to a multi-degree of freedom system is thereby defined through the following system of algebraic equations

$$\mathbf{M}^e\ddot{\mathbf{d}}^e + \mathbf{K}^e\mathbf{d}^e - \mathbf{f}^e = 0 \quad (30)$$

where the matrices $\mathbf{M}^e$ and $\mathbf{K}^e$ represent, respectively, the mass and the stiffness element matrices and $\mathbf{f}^e$ the element vector of external forces; $\mathbf{d}^e$ represents the element nodal displacements, having 14 components, corresponding to 7 degrees of freedom considered for each end, being written by

$$\mathbf{d}^e = \begin{bmatrix} \mathbf{d}_1^e & \mathbf{d}_2^e \end{bmatrix}^T \quad (31)$$

where $\mathbf{d}_1^e$ and $\mathbf{d}_2^e$ are defined as follows

$$\begin{aligned} \mathbf{d}_1^e &= \begin{bmatrix} u_1^e & w_{y1}^e & w_{y1}'^e & w_{z1}^e & w_{z1}'^e & w_{\varphi 1}^e & w_{\varphi 1}'^e \end{bmatrix}^T \\ \mathbf{d}_2^e &= \begin{bmatrix} u_2^e & w_{y2}^e & w_{y2}'^e & w_{z2}^e & w_{z2}'^e & w_{\varphi 2}^e & w_{\varphi 2}'^e \end{bmatrix}^T \end{aligned} \quad (32)$$

The beam element is shown in Fig. 5. The displacements represented by the three arrows are the twist curvatures, expressed as first derivative of the twist angle for each end node because Vlasov's theory is considered.

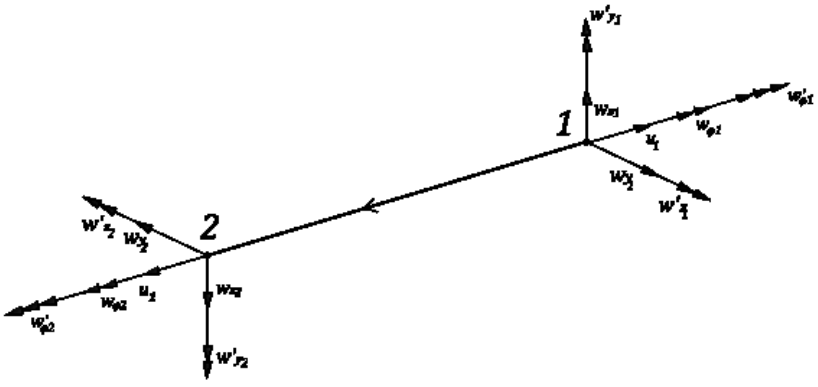

Fig. 5 Beam element and generalized degrees of freedom.

The stiffness components associated with the torsional degree of freedom are written for the reference frame with the point *P* as the respective origin as follows

$$\mathbf{K}_{\varphi}^{e} = \mathbf{K}_{\varphi 1}^{e} + \mathbf{K}_{\varphi 2}^{e} + \mathbf{K}_{\varphi 3}^{e} + \mathbf{K}_{\varphi 4}^{e} \tag{33}$$

where the different components refer to the axial, bending in the (*x*,*z*), (*x*,*y*) plans and torsion contribution considering the coupled effects. These components are given by

$$\mathbf{K}_{\varphi 1}^{e} = \int_{-1}^{1} \left[\frac{8}{\left(L^{e}\right)^{3}} \left(\frac{d^{2}\mathbf{H}_{\varphi}^{e}}{d\xi^{2}} \right)^{T} ES_{\omega}^{P} \left(\frac{d\mathbf{N}^{e}}{d\xi} \right) \right] u_{x}^{e} \frac{L^{e}}{2} d\xi \tag{34}$$

$$\mathbf{K}_{\varphi 2}^{e} = \int_{-1}^{1} \left[\frac{16}{\left(L^{e}\right)^{3}} \left(\frac{d^{2}\mathbf{H}_{\varphi}^{e}}{d\xi^{2}} \right)^{T} EI_{\omega y}^{P} \left(\frac{d^{2}\mathbf{H}_{y}^{e}}{d\xi^{2}} \right) \right] u_{y}^{e} \frac{L^{e}}{2} d\xi \tag{35}$$

$$\mathbf{K}_{\varphi 3}^{e} = \int_{-1}^{1} \left[\frac{16}{\left(L^{e}\right)^{4}} \left(\frac{d^{2}\mathbf{H}_{\varphi}^{e}}{d\xi^{2}} \right)^{T} EI_{\omega z}^{P} \left(\frac{d^{2}\mathbf{H}_{y}^{e}}{d\xi^{2}} \right) \right] u_{z}^{e} \frac{L^{e}}{2} d\xi \tag{36}$$

$$\mathbf{K}_{\varphi 4}^{e} = \int_{-1}^{1} \left[\frac{16}{\left(L^{e}\right)^{4}} \left(\frac{d^{2}\mathbf{H}_{\varphi}^{e}}{d\xi^{2}} \right)^{T} EI_{\omega\omega}^{P} \left(\frac{d^{2}\mathbf{H}_{\varphi}^{e}}{d\xi^{2}} \right) \right] u_{\varphi}^{e} \frac{L^{e}}{2} d\xi \tag{37}$$

As done for the elements stiffness matrix, the mass components associated with the torsional degree of freedom are written for the same reference frame as follows

$$\mathbf{M}_{\varphi}^{e} = \mathbf{M}_{\varphi 1}^{e} + \mathbf{M}_{\varphi 2}^{e} + \mathbf{M}_{\varphi 3}^{e} + \mathbf{M}_{\varphi 4}^{e} \tag{38}$$

where the different components refer to the same contributions considered for the stiffness matrix. The components of the mass matrix are given by

$$\mathbf{M}_{\varphi 1}^{e} = \int_{-1}^{1} \left[\frac{2}{L^{e}} \left(\frac{d\mathbf{H}_{\varphi}^{e}}{d\xi} \right)^{T} \rho S_{\omega}^{P} N^{e} \right] \ddot{u}_{x}^{e} \frac{L^{e}}{2} d\xi \tag{39}$$

$$\mathbf{M}_{\varphi 2}^{e} = \int_{-1}^{1} \left[\frac{4}{\left(L^{e}\right)^{2}} \left(\frac{d\mathbf{H}_{\varphi}^{e}}{d\xi} \right)^{T} \rho I_{\omega y}^{P} \left(\frac{d\mathbf{H}_{y}^{e}}{d\xi} \right) - \left(\mathbf{H}_{\varphi}^{e} \right)^{T} \rho S_{z}^{P} \mathbf{H}_{y}^{e} \right] \ddot{u}_{y}^{e} \frac{L^{e}}{2} d\xi \tag{40}$$

$$\mathbf{M}_{\varphi 3}^{e} = \int_{-1}^{1} \left[\frac{4}{\left(L^{e}\right)^{2}} \left(\frac{d\mathbf{H}_{\varphi}^{e}}{d\xi} \right)^{T} \rho I_{\omega z}^{P} \left(\frac{d\mathbf{H}_{z}^{e}}{d\xi} \right) + \left(\mathbf{H}_{\varphi}^{e} \right)^{T} \rho S_{y}^{P} \mathbf{H}_{z}^{e} \right] \ddot{u}_{z}^{e} \frac{L^{e}}{2} d\xi \tag{41}$$

$$\mathbf{M}_{\varphi 4}^{e} = \int_{-1}^{1} \left[\frac{4}{\left(L^{e}\right)^{2}} \left(\frac{d\mathbf{H}_{\varphi}^{e}}{d\xi} \right)^{T} \rho I_{\omega\omega}^{P} \left(\frac{d\mathbf{H}_{\varphi}^{e}}{d\xi} \right) + \left(\mathbf{H}_{\varphi}^{e} \right)^{T} \rho \left(I_{y}^{P} + I_{z}^{P} \right) \mathbf{H}_{\varphi}^{e} \right] \ddot{u}_{\varphi}^{e} \frac{L^{e}}{2} d\xi \tag{42}$$

The coupling between torsional and flexural behaviour occurs due to inertial effects, Eqs. (24), (25) and (26), even if the equilibrium equations are referred to the shear centre and the centroid of the cross-section. In the sequel, the beam element is derived in a coupled form by considering a

single axis. By doing so the compatibility of displacements between elements is simplified. In fact, although being possible, Gunnlaugsson and Pedersen (1982), the compatibility between beam elements that were formulated considering both shear centre and centroid axes is not so straightforward to implement.

Furthermore, the obtained coupled lateral-torsional vibration modes can be directly represented by the displacements of the corresponding axis, allowing a clear understanding of the vibration phenomena and the evaluation of the modal participation factors.

Therefore, and since it is not possible to uncouple the beam dynamic equations, the finite element was derived by referring the equations to a single axis, assuming thereby a coupled form. This formulation has the advantage of considering the compatibility between elements in a simplified procedure since the nodal displacements are referred to a single axis. The element stiffness, $\mathbf{K}^e$, mass $\mathbf{M}^e$ and the vector of external forces $\mathbf{f}^e$ written in Eq. (30) are obtained considering the element axis coincident with the elastic centre axis *C*, being given in the appendix.

This formulation allows to define the displacement field, the stress distribution and the boundary conditions of the element referred to the same axis and take into account the coupling between bending and torsion, as represented for a mono-symmetric beam (Fig. 4).

3.2 Structural dynamic analysis

The dynamic analysis of the combined flexural-torsional vibration for general multi-spans bridges is considered through the previously developed model.

3.2.1 Free vibrations of the system

The finite element method is used in the sequel for solving the vibration problem for a continuous straight beam structure. The dynamic equilibrium of the system is described by a vectorial equation, written for the undamped vibration in the following form

$$\mathbf{M}\ddot{\mathbf{v}} + \mathbf{K}\mathbf{v} = 0 \tag{43}$$

where **M** and **K** are respectively the mass and stiffness matrices of the multi-degrees of freedom system. Notice that these matrices are obtained assembling the element property matrices (presented in section 2) that compose the whole system using the finite element method techniques. If harmonic functions are considered for the time-variation of the displacements *v(t)* the Eq. (43) can be written as

$$\left[\mathbf{K} - p^2\mathbf{M}\right]\hat{\mathbf{v}} = 0 \tag{44}$$

where *p* is the radian frequency and $\hat{\mathbf{v}}$ is the *amplitude* of the displacement vector. The Eq. (44) represents an eigenvalue problem, being the corresponding *N* roots the frequencies of the respective modes of vibration.

3.2.2 Forced vibrations of the system

The orthogonality properties of the normal coordinates may be used to simplify the equations of motion of the system. The general form of the dynamic equations for the damped system is given by

$$\mathbf{M}\ddot{\mathbf{v}} + \mathbf{C}\dot{\mathbf{v}} + \mathbf{K}\mathbf{v} = \mathbf{f}(t) \tag{45}$$

where ***C*** is the damping matrix of the system and **f**(t) is the time-dependent external load vector. The element damping matrix is calculated *a posteriori* as proportional to the mass and the stiffness matrix by the Rayleigh assumptions, Lisi (2012), so as to satisfy the orthogonality conditions. The Eq. (45) can be written in normalized coordinates to obtain an independent SDOF equation for each vibrational mode of the structure as follows

$$M_n\ddot{Y}_n + C_n\dot{Y}_n + K_nY_n = F_n(t) \tag{46}$$

In Eq. (46) Y_n is the scalar modal coordinate, i.e., the modal amplitude at time t, being the structure property matrices normalized with respect to the n-vibrational mode and thus represented with the subscript n. The displacements can now be expressed in geometric coordinates by the modal superposition method, leading to

$$v(t) = \phi_1 Y_1 + \phi_2 Y_2 + ... + \phi_n Y_n + ... \tag{47}$$

being ϕ_n the shape vector of the n-th vibration mode.

An eccentrically concentrated moving load traveling with a constant velocity is considered in the thin-walled beam model. The mass of the moving load is considered to be small when compared with the mass of the thin-walled structure and thus the corresponding inertial effects are neglected, Fryba (1999).

4. Benchmarking of the model

The developed model is applied to (i) the analysis of free vibrations of thin-walled beams, evaluating the natural frequencies and the corresponding vibrational modes, and (ii) to the analysis of beams submitted to a moving load. Towards an evaluation of the model performance, a comparison with models reported in the literature was made, namely the formulation of Prokic (2005) regarding the evaluation of coupled natural frequencies and the analytical solution of Michaltsos *et al.* (2005) for a moving load analysis including the cross-section warping in a simple supported beam. A comparison with the pioneer work of Gere (1954) was also performed, allowing to verify an excellent agreement between results, which however are not presented in this paper, but can be found in Lisi (2012).

4.1 Coupled flexural-torsional free vibrations

Whenever the centroid and the shear centre do not coincide, the free vibration of a beam with a non-symmetric cross-section results in a coupled vibration of flexural and torsional modes. The analytical solution of the coupled equilibrium equations towards the evaluation of the natural frequencies becomes more difficult and cumbersome to obtain for general support conditions. Conversely, the numerical model derived in section 3 is an efficient form of evaluating coupled natural frequencies for more general boundary conditions, in particular those corresponding to continuous bridge girders.

The coupled frequencies of a simple supported beam with a double-T cross-section (represented in Fig. 6 with the dimensions given in Table 1) are obtained analytically from the formulation presented in 2 by considering the equilibrium equations referred to the elastic centre axis and neglecting rotary inertial effects, since its relevance for lower modes of vibration can be considered reduced. Similarly to Timoshenko (1974), Gere (1954) and Prokic (2005), the

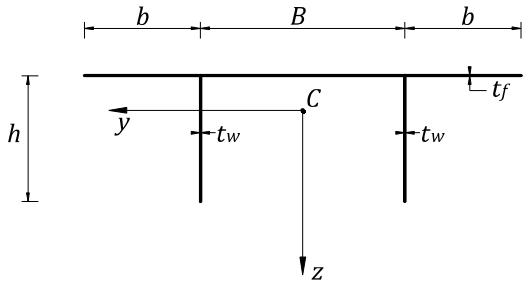

Fig. 6 Double-T cross-section layout

Table 1 Double-T cross-sectio dimensions

B [m]	0.45	t_w [m]	t_f [m]	h [m]
6.65	3.33	0.80	0.35	3.03
A [m^2]	I_y [m^4]	I_z [m^4]	$I_{\omega\omega}$ [m^6]	K [m^4]
9.51	9.16	122.37	110.14	1.17

displacement components are defined by lengthwise sine functions (having n multiples of the beam span as wavelengths, $n\pi x/L$) in compliance with the beam boundary conditions (simple-supported). For each wavelength n=1, 2, 3, two coupled natural frequencies are obtained, which correspond to modes with a predominantly flexural and with a prevalently torsional behaviour.

The coupled natural frequencies obtained for the three wavelengths from the derived formulation are compared with the formulations of Prokic (2005) ("exact" approach) and of Michaltsos *et al.* (2005), which neglects rotary inertial effects. Two numerical values of frequencies are given for each wavelength n; the lowest value (which is lower than the corresponding uncoupled value) represents a response predominantly torsional, while the highest value (higher than the corresponding uncoupled value) is prevalently flexural, Gere and Lin (1958). The developed formulation allows to obtain "exact" values of frequencies for each wavelength n as it can be inferred from Table 2, while the error associated with *Michaltsos's* obtained frequencies, although negligible for the first frequency, increases with n and is higher for the prevalently flexural frequencies. This is due to the fact that rotary inertial effects are neglected in Michaltsos *et al.* (2005): the second frequency associated with n=3, where prevalently flexural motion is involved, is 23.7% higher then the exact value. (the error *Michaltsos's* formulation is evaluated by $[(f_e-f_M)/f_M]/100$, represented in Table 2 as "Dimensionless difference", f_e is the exact frequency and f_M is obtained frequency).

The finite element derived in section is applied to the free vibration analysis of beams so as to efficiently consider more general boundary conditions. The accuracy of the solution in terms of natural frequencies is verified for the 1st and 2nd vibrational modes of the double-T simple supported beam; the results obtained with numerical models with 1, 2, 4 and 8 finite elements are presented in Table 3, being verified a good agreement between results and a convergence to the exact values as the model is refined by increasing the number of elements. A small number of elements for the model increases the beam stiffness and hence the frequency values obtained by the numerical model are higher than the exact values; nevertheless, good results in terms of convergence are attained; frequencies obtained from a model with only 4 elements for the first and second mode are, respectively, 0.015% and 0.026% higher than the corresponding exact values.

Table 2 Mode vibration frequencies for the S-S beam with double coupling

Wavelength	**n=1**		**n=2**		**n=3**		
Freq. [Hz]	2.74	8.60	8.64	31.75	18.19	64.16	Prokic (exact)
	2.75	8.85	8.69	35.29	18.43	79.36	Michaltsos
	0.14	2.90	0.56	11.15	1.27	23.68	Dimensionless difference [%]
	2.74	8.60	8.64	31.74	18.19	64.16	**Presented formulation**

Table 3 Covergence rate of frequencies for the 1st and 2nd vibration modes

Developed finite element					
Vibr. Mode Freq.	1 el.	2 el.	4 el.	8 el.	
1 mode [Hz]	2.9076	2.7492	2.7439	2.7435	Exact: 2.7435Hz
	5.981	0.208	0.015	0.000	**Dimensionless difference** [%]
2 mode [Hz]	9.5364	8.6356	8.6043	8.6022	Exact: 8.6021Hz
	10.861	0.389	0.026	0.001	**Dimensionless difference** [%]

The warping of a thin-walled cross-section increases the natural frequency of a beam, being therefore a relevant effect to consider in a dynamic analysis, Gere (1958), Banerjee *et al.* (1996). Towards the evaluation of the cross-section warping influence on the structure dynamic response, the derived finite element was adopted for evaluating coupled natural frequencies for different values of the warping stiffness and for three different boundary conditions: (i) SS - simple-supported; (ii) CS - clamped/simple supported and (iii) CC - clamped beam. (the warping degree-of-freedom is free for a simple supported condition and restrained for a clamped support). The results are presented through two non-dimensional parameters: (i) p/p_{SS} (x) that represents the frequency increase expressed as a ratio between the frequency of a generally supported beam, p, and the frequency of a simple supported beam, p_{SS}; and (ii) a relation between torsional and warping stiffness considered by a coefficient defined as follows

$$\kappa = \sqrt{\frac{GKL^2}{EI_{\omega\omega}}} \tag{48}$$

where L is the beam length. The frequency ratio is obtained by solving the eigenvalue problem of Eq. (44) of the numerical model by taking in account the respective boundary conditions. Frequencies of the first and second modes of vibration are represented in a semi-logarithmic scale in Fig. 7 as functions of the dimensionless parameter κ for each vibrational mode.

Lower values of κ correspond to a more notorious increase of the respective frequency; e.g., for a beam with warping restrained at both ends the ratio between frequencies, p/p_{SS} (x), is up to 230% for the first vibrational mode. Conversely, whenever the torsional response of the cross-section is mainly due to pure *Saint-Venant* torsion κ>15 the relation between frequencies, p/p_{SS} (κ), is lower and the warping influence on increasing the frequency diminishes. It can be inferred from these results that the warping is more relevant for thin-walled cross-sections with an open profile than for closed cross-sections, being the boundary conditions restraining warping an important factor to consider since it significantly increases the beam natural frequencies. However, the increase of modal frequency for higher vibration modes is smaller, even for the cases of pure warping torsion; in fact, for higher modes of vibration, the stiffness is not as a much affected by restraining warping.

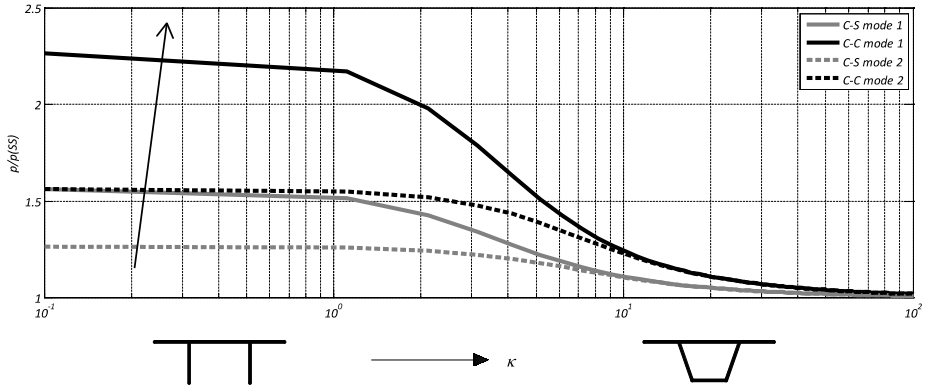

Fig. 7 Influence of boundary conditions on the 1st and 2nd mode frequencies

Table 4 Maximum midspan displacements with load speed v=20 m/s

max $u_y(L/2)$ [mm]	max φ $(L/2)$ [rad*10^{-3}]	
−0.31	0.21	Michaltsos *et al.* (2005)
−0.31	0.22	Present model
−0.2147%	−3.3833%	**Dimensionless difference** [%]

4.2 Dynamic response due to an eccentric moving load

The developed model was applied to the analysis of a simple supported thin-walled beam submitted to an eccentric moving load; the beam has a span with $L=50$ m and a mono-symmetric double-T cross-section. This example was solved analytically in Michaltsos *et al.* (2005) and is adopted herein for comparison purposes. The cross-section geometry is thus equal to that considered in Michaltsos *et al.* (2005).

The formulation of Michaltsos *et al.* (2005) derives a set of beam governing equations that includes the cross-section warping, considering the cross-section shear centre for the torsional behaviour and the cross-section elastic centre for the flexural behaviour. The beam response to a concentrated moving load P_z acting eccentrically in the beam cross-section was obtained by considering modal solutions defined lengthwise by sinusoidal functions and using Duhamel's integral.

The midspan displacement u_y and the cross-section torsion φ were obtained for different moving load velocities v, magnitudes P_z and eccentricities e. A comparison between the maximum midspan displacement u_y and torsion φ obtained from the developed model and from the formulation of Michaltsos *et al.* (2005) is presented in Tables 4 and 5 for a moving load P_z=1500 kp (kp-kilopond, 1 kp=9.8 N) acting with an eccentricity of e=1m and for the velocities of v=20 ms^{-1} and v=40 ms^{-1}. The results obtained by the developed numerical model are in a good agreement with those corresponding to the formulation of Michaltsos *et al.* (2005); (a dimensionless difference determined as $[(f_M-f)/f]/100$ where f_M is the displacement value obtained by Michaltsos's equations, while f corresponds to the frequency obtained using the developed model). The different values are mainly due to the neglected rotary inertia in the governing equations derived by Michaltsos *et al.* (2005).

Table 5 Maximum midspan displacements with load speed v=40 m/s

max $u_y(L/2)$ [mm]	max φ $(L/2)$ [rad*10^{-3}]	
−0.46	0.31	Michaltsos *et al.* (2005)
−0.47	0.32	Present model
−2.4737%	−3.0858%	**Dimensionless difference** [%]

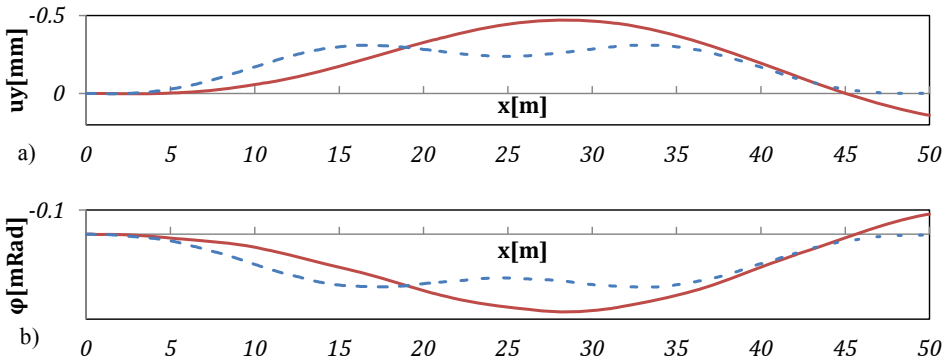

Fig. 8 Dynamic influence lines at the midspan point: 20 m/s (dashed) and 40 m/s (cont.): (a) displacement u_y; (b) rotation φ

5. Application to the dynamic analysis of a bridge girder

The finite element derived in section 3 that includes the cross-section warping as an additional degree-of-freedom and is formulated with reference to a single axis coinciding with the beam elastic centre, allows to efficiently perform the dynamic analysis of continuous bridge girders submitted to an eccentric moving load. This model represents a novel approach for the dynamic analysis of bridges through a thin-walled beam model when compared with other formulations reported in the literature. In fact, regarding the dynamic response to an eccentric moving load, the work of Michaltsos *et al.* (2005), being based on an analytical formulation, is not efficient to analyse a continuous beam. On the other hand, other works that have studied the bridge dynamics have not included warping, Garinei and Risitano (2008).

A continuous concrete bridge with three spans (30 m+40 m+30 m), represented in Fig. 9, submitted to a vertical force moving at constant speed and acting with an eccentricity regarding the cross-section shear centre is analysed by the developed numerical model. Two types of cross-sections are considered: (i) the double-T cross-section previously analysed in section 4.1, which is depicted in Fig. 6, having the characteristics given in Table 1 and (ii) a closed cross-section with the geometry represented in Fig. 10 with the properties represented in Table 5; these two cross-sections are made of a concrete with an elastic modulus of 32 GPa and have been considered so as to have an equivalent flexural stiffness. The analysis is performed numerically by the derived finite element, considering a model discretization with 100 elements for the central span and 75 elements for the lateral spans. The natural frequencies are obtained by the solution of the eigenvalue problem stated in Eq. (44), where both the stiffness and the mass matrices take into account the warping degree of freedom, being the mass associated with the railway bridge self-weight and a superimposed dead load of 85 kN/m. The railway traffic is modeled by a single vertical load

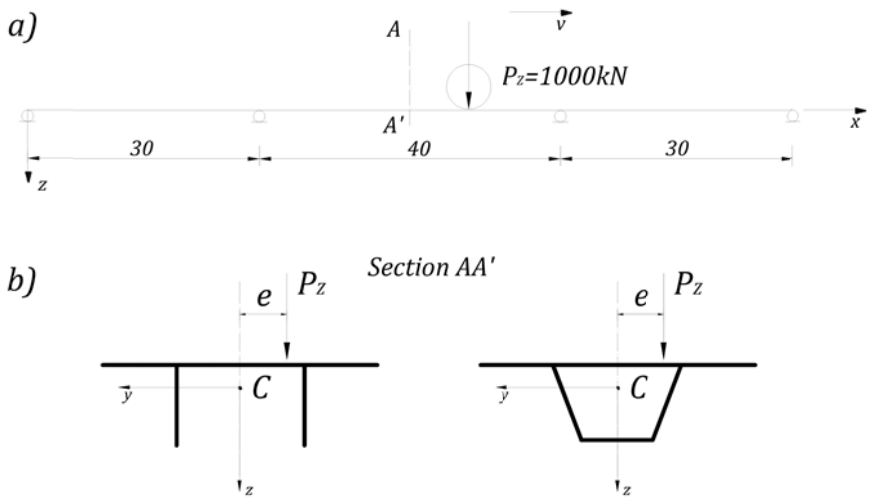

Fig. 9 Longitudinal beam-like model (a) and layout of the cross-section analyzed (b)

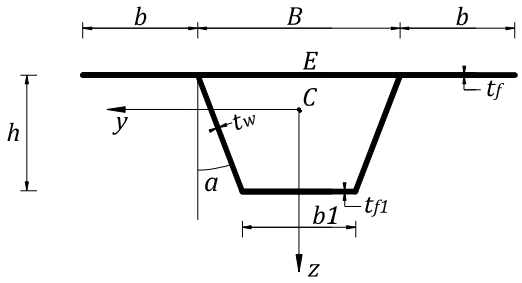

Fig. 10 Box girder section layout

Table 5 Cross-section layouts and geometrical properties

B [m]	b [m]	t_w [m]	t_f [m]	t_{fl} [m]		h [m]
7.30	3.00	0.50	0.35	0.30	23	2.28
A [m^2]	I_y [m^4]	I_z [m^4]	$I_{\omega\omega}$ [m^6]	K [m^4]		
8.74	7.84	97.50	12.06	17.14		

P_z=1000 kN, which is admitted to move at constant speed and with a transverse eccentricity of e=2.5 m relatively to the cross-section shear-centre, which corresponds to the railway track position.

5.1 Free vibration analysis

The natural frequencies obtained from the numerical model are presented in Table 6 for both cross-sections, being identified the corresponding vibrational mode. Not all the vibration modes are considered relevant for the analysis; in fact, the EN 1990-A2 refers that for the dynamic analysis of a bridge it is sufficient to consider the frequencies up to 30 Hz, therefore, for this example, only the first 15 vibration modes are considered.

Table 6 Mode vibration frequencies for the bridge model

	Double-T section		Box girder section	
Mode	**Freq. [Hz]**	**Major modal participation**	**Freq. [Hz]**	**Major modal participation**
1	**3.97**	u_z motion	**3.79**	u_z motion
2	**4.81**	Coupled u_y-(φ) motion	**6.19**	u_z motion
3	**6.49**	u_z motion	**7.43**	u_z motion
4	**7.37**	Coupled u_y-(φ) motion	**9.08**	u_x motion
5	**7.79**	u_z motion	**10.68**	Coupled u_y-(φ) motion
6	**8.52**	Coupled u_y-(φ) motion	**14.16**	u_z motion
7	**9.08**	u_x motion	**14.22**	Coupled u_y-(φ) motion
8	**14.84**	u_z motion	**14.37**	Coupled u_y-(φ) motion
9	**15.81**	Coupled u_y-(φ) motion	**17.01**	Coupled u_y-(φ) motion
10	**17.34**	Coupled u_y-(φ) motion	**21.50**	u_z motion
11	**22.51**	u_z motion	**22.32**	Coupled u_y-(φ) motion
12	**23.64**	Coupled u_y-(φ) motion	**23.44**	u_z motion
13	**24.55**	u_z motion	**26.17**	Coupled u_y-(φ) motion
14	**25.61**	Coupled u_y-(φ) motion	**27.25**	u_x motion
15	**27.25**	u_x motion	**29.80**	Coupled u_y-(φ) motion

The behaviour of the two cross-sections is significantly different, in that for the open cross-section the coupled vibrational modes occur for lower values of frequency (namely, the 2nd mode, with 4.81 Hz), whereas for the closed section the coupled vibrations correspond to higher natural frequencies (the first three frequencies are all given by bending motion in the vertical plane, being the coupled mode associated with a frequency of 10.68 Hz).

5.2 Forced vibration analysis

The dynamic response of the bridge due to an eccentric moving load P_z is obtained from a modal analysis of the numerical model, adopting the *Newmark* method for the time integration procedure with an interval of $\Delta t[s]=0.01T_1$. The double-T and the box girder cross-section are considered in the analysis, being possible to highlight its influence on the bridge dynamic response. A material damping corresponding to a coefficient of 1% is considered, being derived a proportional damping matrix according with Rayleigh procedure, Lisi (2012). Five different speeds of the load passage are considered in the analysis, being the considered values usual in the design of high-speed railway bridges; a minimum speed of 200 km/h and a maximum speed of 350 km/h, which corresponds to a design speed of 420 km/h is considered.

A dynamic analysis is performed by computing the influence lines at AA' section, considering the double-T section of Fig. 9, for the rotation of the cross-section torsion φ and for the horizontal and vertical displacements, u_y and u_z, respectively. The results (dynamic influence lines) for the double-T section are represented in Fig. 11, being in Fig. 12 the correspondent dynamic lines of the box girder section.

A dynamic influence line can be considered to represent an index of structural flexibility whenever the bridge is submitted to a load moving lengthwise along the bridge girder. The maximum values of midspan vertical displacements are obtained for speed values of 300 km/h and

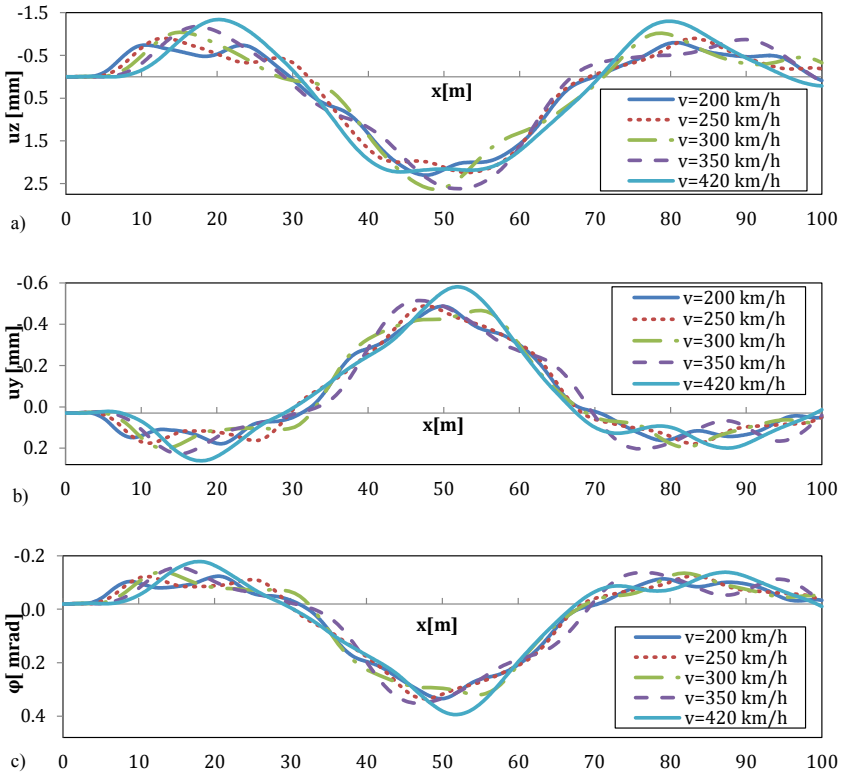

Fig. 11 Dynamic influence lines at the section AA' (double-T section): displacement (a) u_z and (b) u_y; (c) rotation φ

350 km/h, being the vertical deflection of the box section similar to those obtained for the open section, Figs. 11 and 12, since the rotary inertia of both cross-sections around the y-axis are of the same order of magnitude.

The effect of warping characterizes the torsional response of the double-T section as it can be verified in Fig. 11; the dynamical response regarding the values of torsion and horizontal displacement, φ and u_y respectively, have more oscillations than the vertical displacements of u_z as can be observed from the corresponding influence lines. The dynamic response of the bridge with the closed cross-section has an increased oscillation pattern (by comparison with the results of the double-T cross-section), which is verified through the influence line of φ represented in Fig. 12; this fact is a consequence of the higher torsional stiffness of the box girder when compared with the double-T section, which is also represented on the free vibration analysis, table 6.

The different response between the box girder section and double-T section regarding the rotation of torsion, φ, is highlighted in Fig. 13 for speeds of 420 km/h and 200 km/h. Notice that the maximum values of φ at the AA' section for the double-T section are about 4 times higher than those of the box section. In fact, the rotation of torsion of the closed section has maximum values for the loading positioned at the central span, whilst for the open section, which is more prone to warping effects, the higher values of rotation are associated with loads acting at the lateral spans.

The u_y displacements for the double-T section are more relevant in terms of magnitude by

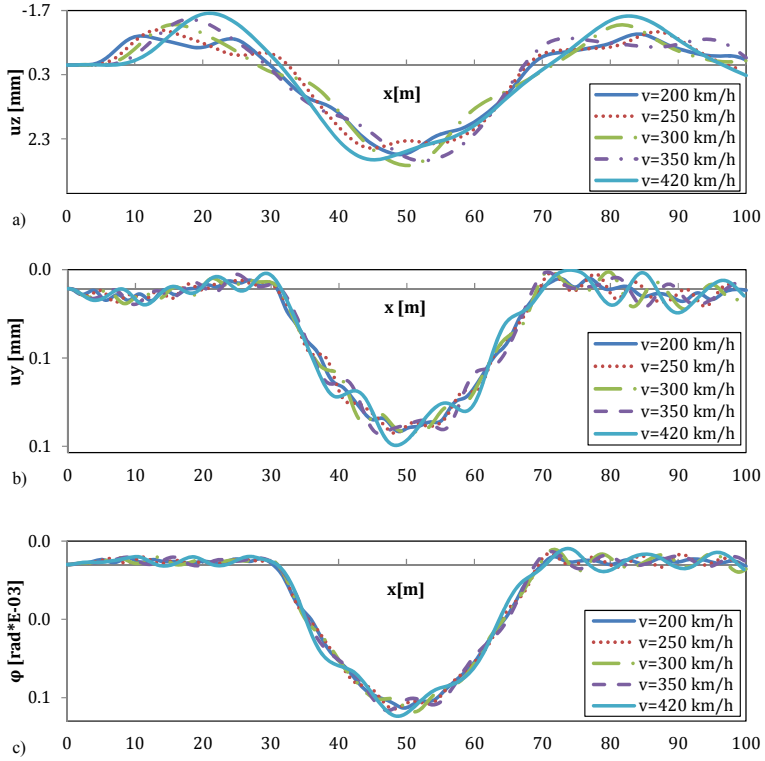

Fig. 12 Dynamic influence lines at the section AA' (Box girder section): displacement (a) u_z and (b) u_y; (c) rotation φ

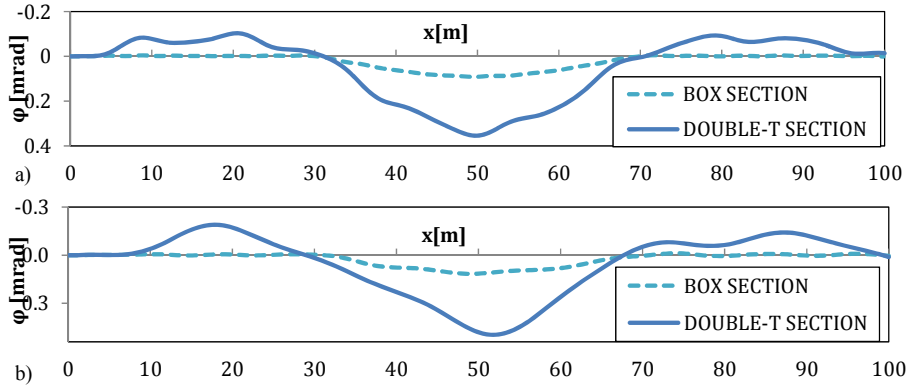

Fig. 13 Twist rotation at the section AA': load speed of (a) 200 km/h and (b) 420 km/h

comparison with those of the box section, being dependent on the torsion's rotation of the section; in fact, the horizontal displacements of the double-T section are about 5 times higher of those of the box girder section.

5.2.1 Effect of speed on the maximum mid-span rotation

The influence of the load speed on the maximum displacements is analysed at the midspan

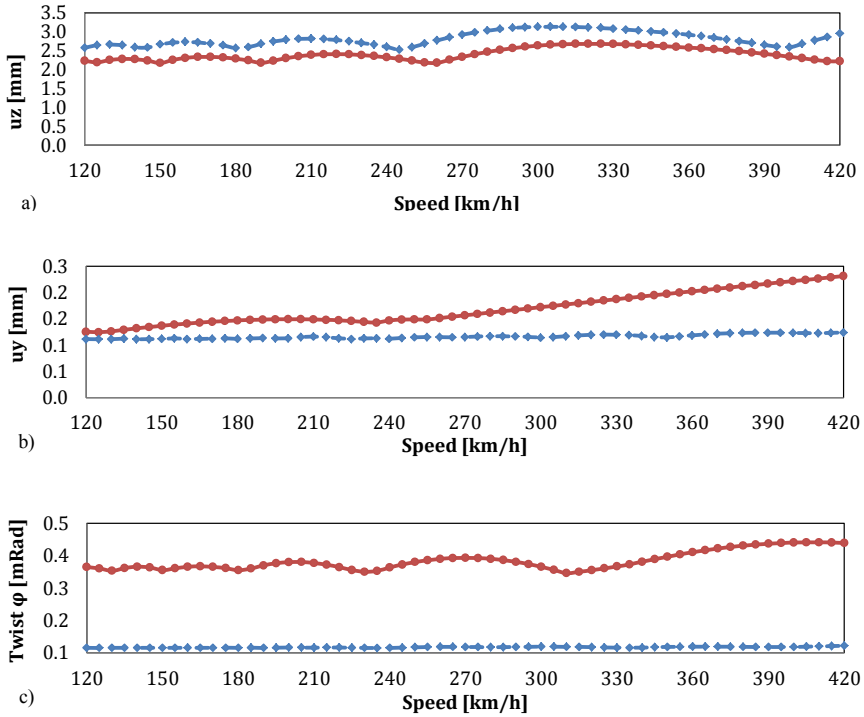

Fig. 14 Maximum generalized displacements at the section (AA'): (a) displacements u_z, (b) u_y and (c) rotation φ. Double-T (cont.) and box girder (dashed) sections

section AA' for a range of speeds between 200 km/h and 420 km/h. The dynamic influence line of each displacement component, u_z, u_y and φ, is obtained for each value of speed, so as to determine the corresponding maximum values, $u_{z,max}$(AA'), $u_{y,max}$(AA') and φ_{max}(AA'). These maximum values of displacements are represented in Fig. 14.

The maximum vertical displacements represented in Fig. 14 ($u_{z,max}$) are similar for both cross-sections since an equivalent bending stiffness was adopted for the cross-sections and also due to a similar dynamical response of the bridge regarding this vibrational mode. Conversely, the cross-section rotation φ_{max} (AA'), which is represented in Fig. 14, has different values for the two types of cross-sections. In fact, for the closed cross-section, the influence of the moving load speed on the maximum rotation is reduced, being the torsion approximately constant for all values of speed. On the other hand, though, the φ_{max} value for the double-T section is variable with the load speed, being the maximum value obtained for a value of 420 km/h; notice that this value of rotation is 4.3 times higher than the correspondent value of a box girder section. The increase of the rotation of torsion φ occurs at higher velocities, in that the corresponding lateral-torsional vibration response has associated higher values of frequency (see table 6).

The horizontal displacements $u_{y,max}$, being coupled with the cross-section rotation, are also different for the two bridge sections compared. Being the prevalently flexural frequencies of vibration for the coupled modes higher than the prevalently torsional ones, the difference between the values of $u_{y,max}$ (AA') for the two types of cross-section (see Fig. 14) is not as significative as in the case of the torsion rotation.

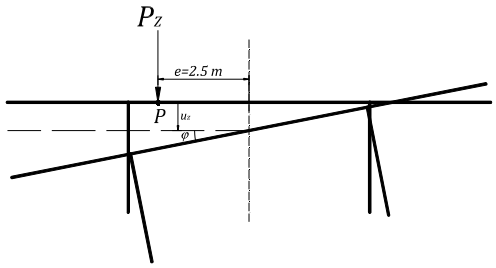

Fig. 15 Sketch of the point P for the double-T section

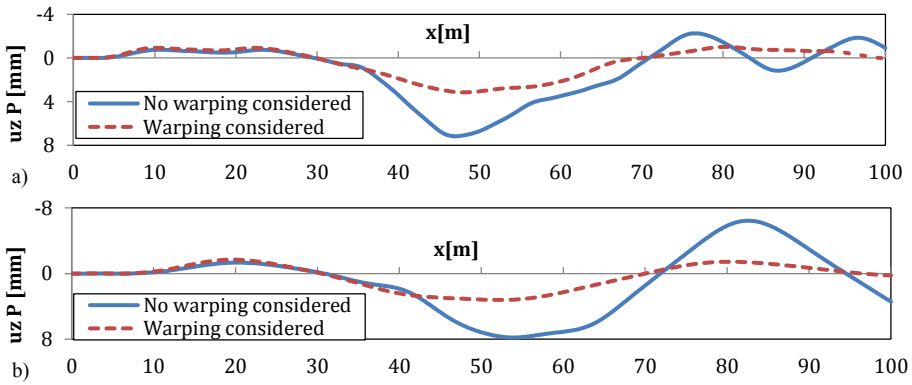

Fig. 16 Dynamic influence line of the displacement u_z^P at the section AA': (a) 200 km/h; (b) 400 km/h

5.2.2 Effect of warping on the open section's rotation

The dynamic effect of the warping deformation is analysed in the sequel for the double-T cross-section of Fig. 9. Towards the evaluation of the warping effect on the bridge dynamic response, the vertical displacement of the cross-section point P, which corresponds to the railway track position and hence has an eccentricity of e=2.5 m in relation to the cross-section shear-centre as depicted in Fig. 15, due to an eccentric moving load of P_z=1000 kN was obtained. Dynamic influence lines were computed for that vertical displacement by two numerical models: (i) a model that considers the finite element derived in section 3, which includes an additional degree-of-freedom representing the cross-section warping, and a conventional beam element that does not consider warping. The results obtained are represented in Figs. 16 for two speeds, 200 km/h and 400 km/h; the maximum vertical displacement $u_z^P(x,t)$ obtained by neglecting the warping is 2.43 and 2.28 times higher than the value obtained when warping was considered for 420 km/h and 200 km/h, respectively. This fact highlights the relevance of warping regarding the dynamical response of bridges with an open cross-section.

5.2.3 Amplification of displacements in dynamic response

The amplification of displacements in dynamic response is evaluated by adopting the developed model to compute static and dynamic influence lines for the displacements of the three-span bridge mid-span cross-section AA' due to moving load P_z=1000 kN with an eccentricity e=2.5 m. The static and dynamic influence lines for the displacements u_y and φ of the section AA' are represented in Fig. 17 for load speeds of 350 km/h and 420 km/h, being possible to observe a

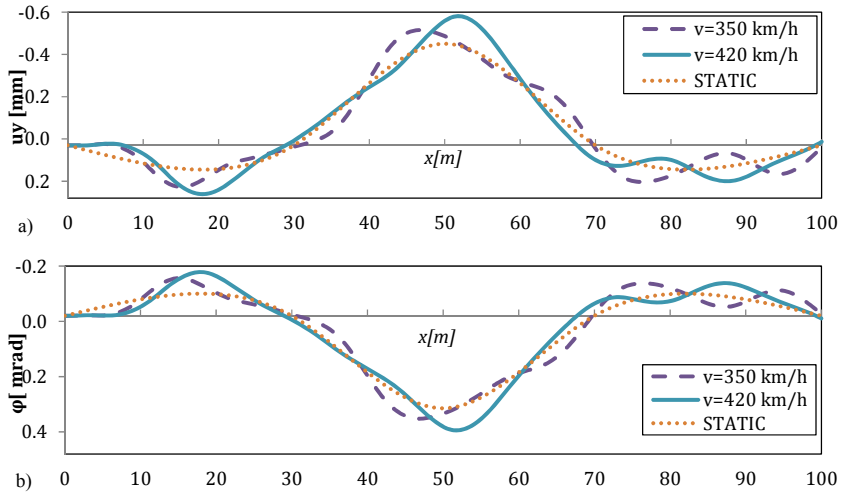

Fig. 17 Influence lines of the displacements at the section AA': (a) disp. u_z; (b) rotation φ

Table 7 Dynamic amplification coefficients

Dynamic factor	$\delta\varphi$	δu_y
350km/h	1.11	1.13
420km/h	1.24	1.27

relevant amplification of displacements.

A coefficient δ_{di} that represent the increase of $\varphi_{\max}$ (AA') and $u_{y,max}$ (AA') due to the dynamic effects produced by the moving load are given for the two considered speeds in Table 7. The coefficients $\delta\varphi$ and δu_y are obtained from $\delta_{di} = u_{di,\max}(AA')/u^S_{di,\max}(AA')$, where u^S_{di} is the static displacement.

5. Conclusions

A beam formulation for the dynamic analysis of thin-walled structures that considers the cross-section warping was presented. The formulation was verified to be accurate on the free vibration analysis of a thin-walled beam, reproducing solutions reported in the literature for single-span beams; the influence of warping on the value of coupled natural frequencies was evaluated for different boundary conditions.

A numerical model based on a derived finite element was adopted so as to obtain the thin-walled beam dynamic response. The finite element has an additional degree of freedom representing the cross section warping, having thus seven degrees of freedom per node; the displacement field (including the component associated with warping) was approximated by Hermite functions. This finite element allowed to efficiently consider general support conditions of beams, easily allowing the analysis of continuous beams and being therefore adopted for the dynamic analysis of a bridge girder.

Furthermore, the analysis of a beam submitted to an eccentric moving load was performed by

the developed numerical model. To the best knowledge of the authors the analysis of a beam submitted to a moving load that involves a lateral-torsional coupled vibration, including the cross-section warping, was carried out analytically and for simple supported beams. The developed finite element allowed to consider the analysis of a thin-walled beam submitted to an eccentric load through a one-dimensional model for general supported conditions, which enabled its application to the dynamic analysis of a bridge girder.

Towards a validation of the numerical model, analytical results of a simple-supported beam submitted to an eccentric moving load were accurately reproduced. The developed model was then adopted for the analysis of a three span continuous bridge, considering two possible types of cross-sections (a double-T and a box girder section) with an equivalent inertia regarding vertical flexure. Coupled lateral-torsional vibrations of the double-T bridge girder were obtained at significantly lower frequencies than those of the closed cross-sections. The bridge girders were submitted to an eccentric moving load, being computed dynamic influence lines of the mid-span displacements for different values of the load speed. The dynamic response of the girder was verified to be affected by the cross-section warping, being particularly relevant for the open cross-section and for higher load speeds.

References

Arpaci, A. and Bozdag, S.E. (2002), "On free vibration analysis of thin-walled beams with nonsymmetrical open cross- sections", *Comput. Struct.*, **80**(7-8), 691-695.

Arpaci, A., Bozdag, S.E. and Sunbuloglu, E. (2003), "Triply coupled vibrations of thin-walled open cross-section beams including rotary inertia effects", *J. Sound Vib.*, **260**, 889-900.

Attard, N.A. (1987), "A direct method of evaluating the warping properties of thin-walled open and closed profiles", *Thin Wall. Struct.*, **5**(5), 351-364.

Banerjee, J.R. (1989), "Coupled bending-torsional dynamic stiffness matrix for beam elements", *Int. J. Numer. Method. Eng.*, **28**, 1283-1298.

Banerjee, J.R. and Williams, F.W. (1992), "Coupled bending-torsional dynamic stiffness matrix for Timoshenko beam elements", *Comput. Struct.*, **42**, 301-310.

Banerjee, J.R. and Guo S. and Howson, W.P. (1996), "Exact dynamic stiffness matrix of a bending torsion coupled beam including warping", *Comput. Struct.*, **59**, 613-621.

Banerjee, J.R. (1997), "Dynamic stiffness formulation for structural elements: A general approach", *Comput. Struct.*, **63**, 101-103.

Bishop, R.E.D., Cannon, S.M. and Miao, S. (1989), "On coupled bending and torsional vibration of uniform beams", *J. Sound Vib.*, **131**(3), 457-464.

Cedolin, L. (1996), *Torsione e taglio di travi a parete sottile*, Milano, Edizioni Cusl.

Dokumaci, E. (1987), "An exact solution for coupled bending and torsion vibrations of uniform beams having single cross-sectional symmetry", *J. Sound Vib.*, **119**(3), 443-449.

Friberg, P.O. (1983), "Coupled vibration of beams - an exact dynamic element stiffness matrix", *Int. J. Numer. Method. Eng.*, **19**, 479-493.

Friberg, P.O. (1985), "Beam Element Matrices Derived from Vlasov's theory of open thin-walled elastic beams", *Int. J. Numer. Method. Eng.*, **21**, 1205-1228.

Fryba, L. (1999), *Vibrations of solids and structures under to moving loads*, Thomas Telford.

Fryba, L. (2001), "A rough assessment of railway bridges for high speed trains", *Eng. Struct.*, **23**, 548-556.

Garinei, A. and Risitano, G. (2008), "Vibrations of railway bridges for high speed trains under moving loads varying in time", *Eng. Struct.*, **30**(3), 724-732.

Gere, J.M. (1954), "Torsional vibrations of beams of thin-walled open cross section", *J. Appl. Mech.*, **25**, 373-378.

Gere, J.M. and Lin, Y.K. (1958), "Coupled vibration of thin-walled beams of open cross section", *J. Appl. Mech.*, **25**, 373-378.
Gunnlaugsson, G.A. and Pedersen, P.T. (1982), "A finite element formulation for beams with thin walled cross-sections", *Comput. Struct.*, **15**(6), 691-699.
Hallauer, W.L. and Liu, R.Y.L. (1982), "Beam bending-torsion dynamic stiffness method for calculation of exact", *J. Sound Vib.*, **85**,105-113.
Chen, H. and Hsiao, K.M. (2008), "Quadruply coupled linear free vibrations of thin-walled beams with a generic open section", *Eng. Struct.*, **30**(5), 1319-1334.
Ichikawa, M., Miyakawa, Y. and Matsuda, A. (2000), "Vibrations analysis of the continuous beam subjected to a moving load", *J. Sound Vib.*, **230**(3), 493-506.
Ju, S.H. and Lin, H.T. (2003), "Resonance characteristics of high-speed trains passing simply supported bridges", *J. Sound Vib.*, **267**, 1127-1141.
Kim, M.Y., Yun, H.T. and Kim, N. (2003), "Exact dynamic and static element stiffness matrices of nonsymmetric thin-walled beam-columns", *Comput. Struct.*, **81**, 1425-1448.
Kim, N. and Kim, M.Y. (2005), "Exact dynamic/static stiffness matrices of non-symmetric thin-walled beams considering coupled shear deformation effects", *Thin Wall. Struct.*, **43**, 701-734.
Lee, S.Y. and Yhim, S.S. (2005), "Dynamic behavior of long-span box girder bridges subjected to moving loads: Numerical analysis and experimental verification", *Int. J. Solid. Struct.*, **42**, 5021-5035.
Li, J. and Su, M. (1999), "The Resonant vibration for a simply supported girder bridge under high-speed trains", *J. Sound Vib.*, **224**(5), 897-915.
Lisi, D. (2012), "A beam finite element including warping", Thesis for Master degree in Structural Engineering, (https://www.politesi.polimi.it/handle/10589/66762?mode=simple).
Michaltsos, G.T., Sarantithou, E. and Sophianopoulos, D.S. (2005), "Flexural-torsional vibration of simply supported open cross-section steel beams under moving loads", *J. Sound Vib.*, **280**, 479-494.
Mohammad, A. R., Farzad, V. and Atefeh E. (2013), "Dynamic response of railway bridges traversed simultaneously by opposing moving trains", *Struct. Eng. Mech.*, **46**(5), 713-734.
Olsson, M. (1985), "Finite Element Modal Coordinate Analysis of structures subjected to moving loads", *J. Sound Vib.*, **99**(1), 1-12.
Olsson, M. (1991), "Finite Element Modal Coordinate Analysis of structures subjected to moving loads", *J. Sound Vib.*, **145**(2), 299-307.
Piccardo, G. and Tubino, F. (2012), "Dynamic response of Euler-Bernoulli beams to resonant harmonic moving loads", *Struct. Eng. Mech.*, **44**(5), 681-704.
Podworna, M. (2011), "Dynamics of a bridge beam under a stream of moving elements. Part 1 - modelling and numerical integration", *Struct. Eng. Mech.*, **38**(3), 283-300.
Podworna, M. (2011), "Dynamics of a bridge beam under a stream of moving elements. Part 2 - numerical simulations", *Struct. Eng. Mech.*, **38**(3), 301-314.
Prokic, A. (2005), "On triply coupled vibrations of thin-walled beams with arbitrary cross-section", *J. Sound Vib.*, **279**(3-5), 21, 723-737.
Prokic, A. (2006), "On fivefold coupled vibrations of Timoshenko thin-walled beams", *Eng. Struct*., **28**(1), 54-62.
Tanaka, M and Bercin, A.N. (1997), "Finite element modelling of the coupled bending and torsional free vibration of uniform beams with arbitrary cross-section", *Appl. Math. Model.*, **21**, 339-344.
Tanaka, M. and Bercin, A.N. (1999), "Free vibration solution for uniform beams of nonsymetrical cross section using Mathematica", *Comput. Struct.*, **71**, 1-8.
Timoshenko, S.P., Young, D.H. and Weaver, W. (1974), *Vibration Problems in Engineering*, Wiley, New York.
Yang, Y.B., Yau, J.D. and Hsu, L.C. (1997), "Vibration of simple beam due to trains moving at highs speeds", *Eng. Struct.*, **19**(11), 936-944.
Vlasov, V. (1961), *Thin-Walled Elastic Beams*, Israel program for scientific translations, Jerusalem.
Zhu, L., Zhao, Y. and Wang, G. (2013), "Exact solution for free vibration of curved beams with variable curvature and torsion", *Struct. Eng. Mech.*, **47**(3), 345-359.

Appendix

A Cross-section properties, stress resultants and external loads

The properties of the cross-section referred to the generic point P are illustrated in Table A.1. Considering the axial displacement and the bending of the beam referred to the elastic centre *C* (Fig. 2) and admitting the rotation around the shear center of the cross-section (A), the stress resultants and the external loads are given by the expressions in Tables A.2 and A.3, respectively.

Table A.1 Geometric properties of the cross-section

	Resultant over the section area
Cross-section area	$A = \int_A dA$
First moments of area	$S_y^P = \int_A (y - y_P)\, dA$ $S_z^P = \int_A (z - z_P)\, dA$
Second moments of area	$I_y^P = \int_A (y - y_P)^2\, dA$ $I_z^P = \int_A (z - z_P)^2\, dA$ $I_{yz}^P = \int_A (y - y_P)(z - z_P)\, dA = I_{zy}^P$
Sectorial moments	$S_\omega^P = \int_A \omega_P(s)\, dA$ $I_{y\omega}^P = \int_A (y - y_P)\, \omega_P(s)\, dA$ $I_{z\omega}^P = \int_A (z - z_P)\, \omega_P(s)\, dA$ $I_{\omega\omega}^P = \int_A \omega_P^2(s)\, dA$
Torsion parameters	Open section $K = \frac{1}{3}\int t^3\, ds$ Closed section $K = \frac{\Omega^2}{\oint \frac{ds}{t}}$

Table A.2 Resultant forces for the degrees of freedom considered

Displacement	Generalized force	**Resultant**
Extension	Axial force	$N = \int_A \sigma_x\, dA$

Table A.2 Continued

Bending in (x,y) plane	Shear force	$V_y = \int_A \tau_{xy}\, dA$
	Bending moment	$M_y = \int_A \sigma_x y\, dA$
Bending in (x,z) plane	Shear force	$V_z = \int_A \tau_{xz}\, dA$
	Bending moment	$M_z = \int_A \sigma_x z\, dA$
Torsion	Torsion moment	$T = \int_A \tau_U\, dA + \int_A \tau_{xs} h_P\, dA$
	Bimoment	$M_\omega = \int_A \omega \sigma_x\, dA$

Table A.3 Resultant beam loads per unit length

Generalized displacements	**Resultant load per unit length**
Extension	$q_x = \int_A p_x\, dA$
Bending in (x,y) plane	$q_y = \int_A p_y\, dA$ $m_y = \int_A p_x (y - y_P)\, dA$
Bending in (x,z) plane	$q_z = \int_A p_z\, dA$ $m_z = \int_A p_x (z - z_P)\, dA$
Torsion	$m_\varphi = \int_A p_z (y - y_P) - p_y (z - z_P)\, dA$ $b = \int_A p_x \omega(s)\, dA$

B Property matrices of the element

The stiffness and mass matrices, both of them symmetric with respect to the diagonal terms, together with the vector of the external nodal forces, can be written by sub-matrices corresponding to the element ends as follows by

$$\mathbf{K}^e = \begin{bmatrix} \mathbf{K}^e_{11} & \mathbf{K}^e_{12} \\ \mathbf{K}^e_{12} & \mathbf{K}^e_{22} \end{bmatrix}, \mathbf{M}^e = \begin{bmatrix} \mathbf{M}^e_{11} & \mathbf{M}^e_{12} \\ \mathbf{M}^e_{12} & \mathbf{M}^e_{22} \end{bmatrix} \text{ and } \mathbf{f}^e = \begin{bmatrix} \mathbf{f}^e_{11} \\ \mathbf{f}^e_{22} \end{bmatrix}$$

being the corresponding components defined as follows:

$$\mathbf{K}_{11}^{e} = \begin{bmatrix}
\frac{EA}{L_e} & \cdot & \cdot & \cdot & \cdot & \cdot & \cdot \\
\cdot & \frac{12EI_y}{L_e} & \frac{6EI_y}{L_e^2} & \cdot & \cdot & \frac{12EI_{\omega y}^C}{L_e^3} & \frac{6EI_{\omega y}^C}{L_e^2} \\
\cdot & \frac{6EI_y}{L_e^2} & \frac{4EI_y}{L_e} & \cdot & \cdot & \frac{6EI_{\omega y}^C}{L_e^2} & \frac{4EI_{\omega y}^C}{L_e} \\
\cdot & \cdot & \cdot & \frac{12EI_z}{L_e^3} & \frac{6EI_z}{L_e^2} & \frac{12EI_{\omega z}^C}{L_e^3} & \frac{6EI_{\omega z}^C}{L_e^2} \\
\cdot & \cdot & \cdot & \frac{6EI_z}{L_e^2} & \frac{4EI_z}{L_e} & \frac{6EI_{\omega z}^C}{L_e^2} & \frac{4EI_{\omega z}^C}{L_e} \\
\cdot & \frac{12EI_{\omega y}^C}{L_e^3} & \frac{6EI_{\omega y}^C}{L_e^2} & \frac{12EI_{\omega z}^C}{L_e^3} & \frac{6EI_{\omega z}^C}{L_e^2} & \frac{12EI_{\omega\omega}^C}{L_e^3}+\frac{36GK}{30L_e} & \frac{6EI_{\omega\omega}^C}{L_e^2}+\frac{3GK}{30L_e} \\
\cdot & \frac{6EI_{\omega y}^C}{L_e^2} & \frac{4EI_{\omega y}^C}{L_e} & \frac{6EI_{\omega z}^C}{L_e^2} & \frac{4EI_{\omega z}^C}{L_e} & \frac{6EI_{\omega\omega}^C}{L_e^2}+\frac{3GK}{30L_e} & \frac{4EI_{\omega\omega}^C}{L_e}+\frac{3GKL_e}{30L_e}
\end{bmatrix}$$

$$\mathbf{K}_{12}^{e} = \begin{bmatrix}
\frac{EA}{L_e} & \cdot & \cdot & \cdot & \cdot & \cdot & \cdot \\
\cdot & -\frac{12EI_y}{L_e} & \frac{6EI_y}{L_e^2} & \cdot & \cdot & -\frac{12EI_{\omega y}^C}{L_e^3} & \frac{6EI_{\omega y}^C}{L_e^2} \\
\cdot & -\frac{6EI_y}{L_e^2} & \frac{2EI_y}{L_e} & \cdot & \cdot & -\frac{6EI_{\omega y}^C}{L_e^2} & \frac{2EI_{\omega y}^C}{L_e} \\
\cdot & \cdot & \cdot & -\frac{12EI_z}{L_e^3} & \frac{6EI_z}{L_e^2} & -\frac{12EI_{\omega z}^C}{L_e^3} & \frac{6EI_{\omega z}^C}{L_e^2} \\
\cdot & \cdot & \cdot & -\frac{6EI_z}{L_e^2} & \frac{2EI_z}{L_e} & -\frac{6EI_{\omega z}^C}{L_e^2} & \frac{2EI_{\omega z}^C}{L_e} \\
\cdot & \frac{12EI_{\omega y}^C}{L_e^3} & \frac{6EI_{\omega y}^C}{L_e^2} & \frac{12EI_{\omega z}^C}{L_e^3} & \frac{6EI_{\omega z}^C}{L_e^2} & -\frac{12EI_{\omega\omega}^C}{L_e^3}+\frac{36GK}{30L_e} & \frac{6EI_{\omega\omega}^C}{L_e^2}+\frac{3GK}{30L_e} \\
\cdot & \frac{6EI_{\omega y}^C}{L_e^2} & \frac{4EI_{\omega y}^C}{L_e} & \frac{6EI_{\omega z}^C}{L_e^2} & \frac{4EI_{\omega z}^C}{L_e} & -\frac{6EI_{\omega\omega}^C}{L_e^2}-\frac{3GK}{30L_e} & \frac{2EI_{\omega\omega}^C}{L_e}-\frac{3GKL_e}{30L_e}
\end{bmatrix}$$

$$\mathbf{K}_{22}^{e}=\begin{bmatrix}
\frac{EA}{L_e} & \cdot & \cdot & \cdot & \cdot & \cdot & \cdot \\
\cdot & \frac{12EI_y}{L_e} & -\frac{6EI_y}{L_e^2} & \cdot & \cdot & \frac{12EI_{\omega y}^{C}}{L_e^3} & -\frac{6EI_{\omega y}^{C}}{L_e^2} \\
\cdot & -\frac{6EI_y}{L_e^2} & \frac{4EI_y}{L_e} & \cdot & \cdot & -\frac{6EI_{\omega y}^{C}}{L_e^2} & \frac{4EI_{\omega y}^{C}}{L_e} \\
\cdot & \cdot & \cdot & \frac{12EI_z}{L_e^3} & -\frac{6EI_z}{L_e^2} & \frac{12EI_{\omega z}^{C}}{L_e^3} & -\frac{6EI_{\omega z}^{C}}{L_e^2} \\
\cdot & \cdot & \cdot & -\frac{6EI_z}{L_e^2} & \frac{4EI_z}{L_e} & -\frac{6EI_{\omega z}^{C}}{L_e^2} & \frac{4EI_{\omega z}^{C}}{L_e} \\
\cdot & \frac{12EI_{\omega y}^{C}}{L_e^3} & -\frac{6EI_{\omega y}^{C}}{L_e^2} & \frac{12EI_{\omega z}^{C}}{L_e^3} & -\frac{6EI_{\omega z}^{C}}{L_e^2} & \frac{12EI_{\omega\omega}^{C}}{L_e^3}+\frac{36GK}{30L_e} & -\frac{6EI_{\omega\omega}^{C}}{L_e^2}-\frac{3GK}{30L_e} \\
\cdot & -\frac{6EI_{\omega y}^{C}}{L_e^2} & \frac{4EI_{\omega y}^{C}}{L_e} & -\frac{6EI_{\omega z}^{C}}{L_e^2} & \frac{4EI_{\omega z}^{C}}{L_e} & -\frac{6EI_{\omega\omega}^{C}}{L_e^2}-\frac{3GK}{30L_e} & \frac{4EI_{\omega\omega}^{C}}{L_e}+\frac{4GKL_e}{30L_e}
\end{bmatrix}$$

$$\mathbf{M}_{11}^{e}=\begin{bmatrix}
J & \cdot & \cdot & \cdot & \cdot & \cdot & \cdot \\
\cdot & AI_y+B & CI_y+D & \cdot & \cdot & AI_{\omega y}^{C} & CI_{\omega y}^{C} \\
\cdot & CI_y+D & EI_y+F & \cdot & \cdot & CI_{\omega y}^{C} & EI_{\omega y}^{C} \\
\cdot & \cdot & \cdot & AI_z+B & CI_z+D & AI_{\omega z}^{C} & CI_{\omega z}^{C} \\
\cdot & \cdot & \cdot & CI_z+D & EI_z+F & CI_{\omega z}^{C} & EI_{\omega z}^{C} \\
\cdot & AI_{\omega y}^{C} & CI_{\omega y}^{C} & AI_{\omega z}^{C} & CI_{\omega z}^{C} & AI_{\omega\omega}^{C}+B & CI_{\omega\omega}^{C}+D \\
\cdot & CI_{\omega y}^{C} & EI_{\omega y}^{C} & CI_{\omega z}^{C} & EI_{\omega z}^{C} & CI_{\omega\omega}^{C}+D & EI_{\omega\omega}^{C}+F
\end{bmatrix}$$

$$\mathbf{M}_{12}^{e}=\begin{bmatrix}
\frac{J}{2} & \cdot & \cdot & \cdot & \cdot & \cdot & \cdot \\
\cdot & -AI_y+\frac{9B}{16} & CI_y-\frac{13D}{22} & \cdot & \cdot & -AI_{\omega y}^{C} & CI_{\omega y}^{C} \\
\cdot & -CI_y+\frac{13D}{22} & -\frac{E+3F}{4}I_y & \cdot & \cdot & -CI_{\omega y}^{C} & -EI_{\omega y}^{C} \\
\cdot & \cdot & \cdot & -AI_z+\frac{9B}{16} & CI_z-\frac{13D}{22} & -AI_{\omega z}^{C} & CI_{\omega z}^{C} \\
\cdot & \cdot & \cdot & CI_z-\frac{13D}{22} & -\frac{E+3F}{4}I_z & -CI_{\omega z}^{C} & -EI_{\omega z}^{C} \\
\cdot & -AI_{\omega y}^{C} & CI_{\omega y}^{C} & -AI_{\omega z}^{C} & -CI_{\omega z}^{C} & -AI_{\omega\omega}^{C}+\frac{9B}{16} & CI_{\omega\omega}^{C}-\frac{13D}{22} \\
\cdot & CI_{\omega y}^{C} & -EI_{\omega y}^{C} & CI_{\omega z}^{C} & -EI_{\omega z}^{C} & -CI_{\omega\omega}^{C}+\frac{13D}{22} & -\frac{E+3F}{4}EI_{\omega\omega}^{C}
\end{bmatrix}$$

$$\mathbf{M}_{22}^{e}=\begin{bmatrix} J & \cdot & \cdot & \cdot & \cdot & \cdot & \cdot \\ \cdot & AI_y+B & -CI_y-D & \cdot & \cdot & AI_{\omega y}^{C} & -CI_{\omega y}^{C} \\ \cdot & -CI_y-D & EI_y+F & \cdot & \cdot & -CI_{\omega y}^{C} & EI_{\omega y}^{C} \\ \cdot & \cdot & \cdot & AI_z+B & -CI_z-D & AI_{\omega z}^{C} & -CI_{\omega z}^{C} \\ \cdot & \cdot & \cdot & -CI_z-D & EI_z+F & -CI_{\omega z}^{C} & EI_{\omega z}^{C} \\ \cdot & AI_{\omega y}^{C} & -CI_{\omega y}^{C} & AI_{\omega z}^{C} & -CI_{\omega z}^{C} & AI_{\omega\omega}^{C}+B & -CI_{\omega\omega}^{C}-D \\ \cdot & -CI_{\omega y}^{C} & -EI_{\omega y}^{C} & -CI_{\omega z}^{C} & -EI_{\omega z}^{C} & -CI_{\omega\omega}^{C}-D & EI_{\omega\omega}^{C}+F \end{bmatrix}$$

The coefficients of the $\mathbf{M}^{e}$ matrix are identified as follows:

$$A=\frac{36\rho}{30L^e};B=\frac{156\rho AL^e}{420};C=\frac{3\rho}{30};D=\frac{22\rho A\left(L^e\right)^2}{420};E=\frac{4\rho L^e}{30};F=\frac{4\rho A\left(L^e\right)^3}{420};J=\frac{\rho AL^e}{3}$$

The vector of nodal forces $\mathbf{f}^{e}$ follows as listed, referring by the subscript 1 and 2 at the beam element ends, respectively:

$$\mathbf{f}_{11}^{e}=\begin{bmatrix} \frac{q_xL^e}{2}-N_1 & \frac{q_yL^e}{2}-m_y-V_{y1} & \frac{q_y\left(L^e\right)^2}{12}-M_{y1} & \frac{q_zL^e}{2}-m_z-V_{z1} & \frac{q_z\left(L^e\right)^2}{12}-M_{z1} & \frac{m_\varphi L^e}{2}-b-T_1 & \frac{q_\varphi\left(L^e\right)^2}{12}-M_{\omega 1} \end{bmatrix}^T$$

$$\mathbf{f}_{22}^{e}=\begin{bmatrix} \frac{q_xL^e}{2}+N_2 & \frac{q_yL^e}{2}+m_y+V_{y2} & \frac{q_y\left(L^e\right)^2}{12}+M_{y2} & \frac{q_zL^e}{2}+m_z+V_{z2} & \frac{q_z\left(L^e\right)^2}{12}+M_{z2} & \frac{m_\varphi L^e}{2}+b+T_2 & \frac{q_\varphi\left(L^e\right)^2}{12}+M_{\omega 2} \end{bmatrix}^T$$